

# Latent Causal Modeling for 3D Brain MRI Counterfactuals

Wei Peng<sup>1</sup>, Tian Xia<sup>3</sup>, Fabio De Sousa Ribeiro<sup>3</sup>, Tomas Bosschieter<sup>1</sup>  
Ehsan Adeli<sup>1</sup>, Qingyu Zhao<sup>2</sup>, Ben Glocker<sup>3</sup>, and Kilian M. Pohl<sup>1</sup>

<sup>1</sup> Stanford University, Stanford, CA 94305

<sup>2</sup> Weill Cornell Medicine, New York, NY 10065

<sup>3</sup> Imperial College London, South Kensington Campus London SW7 2AZ, UK

**Abstract.** The number of samples in structural brain MRI studies is often too small to properly train deep learning models. Generative models show promise in addressing this issue by effectively learning the data distribution and generating high-fidelity MRI. However, they struggle to produce diverse, high-quality data outside the distribution defined by the training data. One way to address the issue is using causal models developed for 3D volume counterfactuals. However, accurately modeling causality in high-dimensional spaces is a challenge so that these models generally generate 3D brain MRIs of lower quality. To address these challenges, we propose a two-stage method that constructs a Structural Causal Model (SCM) within the latent space. In the first stage, we employ a VQ-VAE to learn a compact embedding of the MRI volume. Subsequently, we integrate our causal model into this latent space and execute a three-step counterfactual procedure using a closed-form Generalized Linear Model (GLM). Our experiments conducted on real-world high-resolution MRI data (1mm) provided by the Alzheimer’s Disease Neuroimaging Initiative (ADNI) and the National Consortium on Alcohol and Neurodevelopment in Adolescence (NCANDA) demonstrate that our method can generate high-quality 3D MRI counterfactuals.

## 1 Introduction

Generative AI models have demonstrated great potential to advance numerous medical fields including neuroimaging with 3D brain MRIs [17,22]. The synthesis of medical images is particularly promising for tasks like improving image quality, imputing missing modalities [32], and modeling disease progression [31,7,8]. Recent advances in diffusion probabilistic models (DPMs) [6,24] have played a significant role in this development as they are able to accurately capture the underlying data distributions. This results in synthesized medical images containing a great amount of detail [28,11] that also differ from the training samples [9,30]. However, a key challenge remains to generate realistic samples that are outside the distribution defined by the training data set [10]. Overcoming this challenge is essential to the generalizability of large-scale models [30]. One way to address this shortcoming is by incorporating causality between factors during the generation progress [16]. For example, aging causes a thinning of the cortex that

is accelerated in those with alcohol use disorder or Alzheimer’s disease, which provides a causal interaction not taken into account by statistical models. Here, we propose to integrate causality in the synthesis of 3D brain MRIs so that their generation can be guided by (interventions on) factors such as age, brain regions, and diagnosis.

Specifically we rely on probabilistic Structural Causal Model (SCM) [16,19], which can incorporate the relationships between variables, directed from cause to effect. It indicates that intervening on a cause should lead to changes in the effect, rather than the other way around. This forces the model to consider our premises and assumptions about causality [3]. Contrary to previous SCMs [14,29], we focus on the synthesis of 3D high-fidelity image counterfactuals of structural t1w MRIs. However, building an SCM in a high-dimensional space presents considerable computational challenges, particularly when dealing with voluminous 3D MRIs. To that end, we build a counterfactual model that can learn the causality and perform counterfactual generation in a latent space, which allows us to produce 3D brain MRIs of higher quality than other counterfactual models.

Our model first employs a VQ-VAE [13] to encode the high-dimensional 3D brain MRI into a low-dimensional latent space. We then integrate a causal graphical model [3,15] into this latent space such that interventions are performed in the latent space rather than the observation space (which contains MRIs). The three-step counterfactual procedure, i.e., abduction, action, and prediction, is subsequently achieved by a Generalized linear Model (GLM) [12] with a closed-form solution.

To the best of our knowledge, this is the first work that can perform high-fidelity counterfactual generation of 3D T1w MRIs. Our counterfactual generative model does not only improve interpretability and generative performance but can also diversify (MRI) datasets. Additionally, counterfactual explanations could be key for preventive purposes, as it is inherently capable of showing how one’s brain might change under certain ‘conditions’ such as prolonged substance use. Our main contributions can be summarised as follows:

- We present a novel causal generative modeling framework in a latent space for producing high-fidelity 3D MRI counterfactuals with Markovian probabilistic causal models;
- Our model fulfills all three rungs of Pearl’s ladder of causation and the three-step procedure of the counterfactual generation can be realized efficiently by a novel GLM method;
- We show that our model can perform high fidelity 3D counterfactual generation and also demonstrate its *axiomatic soundness* of our counterfactuals by evaluating its context-level generation.

## 2 Methodology

Our method comprises a two-stage process (outlined in Fig. 1) that performs counterfactual generation of MRIs given attributes, e.g., age and brain regions of interest (ROIs). Given an intervention on (at least) one of these attributes, a

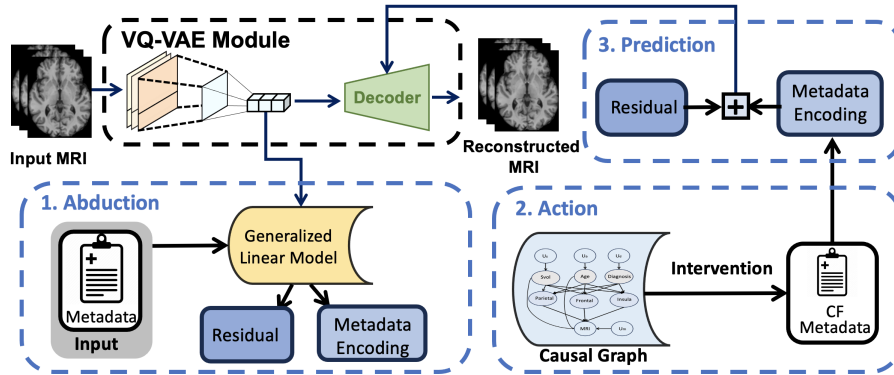


Fig. 1: Architecture of the LSCM for image: Stage I (black box) consists of a VQ-VAE to encode the real 3D MRI to a quantized vector representation. Based on this, in stage II (blue boxes), a Latent SCM is constructed. The three-step procedure of counterfactual inference is achieved by an efficient GLM.

*Deep Structural Causal Model* (DSCM) deploys a causal graph to compute the counterfactual of the attributes. For example, consider a brain MRI scan of an 80-year-old female, from which we extract the attributes `age=80`, `sex=female`, and the two ROI scores `ROI_1_score=0.3` and `ROI_2_score=0.7`. Now to generate the brain MRI at age 50 years old, we intervene and set `age=50`, after which the DSCM computes the counterfactual attribute values, e.g., `age=50`, `sex=male`, `ROI_1_score=0.4` and `ROI_2_score=0.6`. These counterfactual attributes are then used to compute the counterfactual feature embeddings, which are fed into a VQ-VAE decoder [13] in order to generate the corresponding MRI. These two stages are discussed below.

## 2.1 Deep Structural Causal Models

A structural causal model (SCM) [16] is a triple  $\mathcal{M} := \langle U, V, F \rangle$  consisting of two sets of variables: (i) *exogenous* variables  $U = \{u_1, \dots, u_N\}$ ; (ii) *endogenous* variables  $V = \{v_1, \dots, v_N\}$ , and a set of functions known as *causal mechanisms*  $F = \{f_1, \dots, f_N\}$ , which determine the values of the endogenous variables:  $v_k := f_k(\mathbf{pa}_k, u_k)$ , where  $\mathbf{pa}_k$  are the direct causes (*parents*) of  $v_k$ . It is possible to perform an intervention on any  $v_k$  by, e.g., setting it to a constant  $do(v_k := c)$  and thereby disconnect  $v_k$  from its causal parents. SCMs enable the estimation of *counterfactuals* (hypothetical scenarios) via a three-step process: (i) *abduction*: infer the posterior distribution  $P(U | X)$ , which represents the current state of the world; (ii) *action*: perform one or more interventions to obtain a modified model; (iii) *prediction*: infer counterfactual values of the endogenous variables using the modified model and the posterior  $P(U | X)$ .

In this work, we use a deep structural causal model (DSCM) [14] to model the causal relationships between patient attributes such as age, brain regions of

interest, and diagnosis. Following [4], a DSCM uses a conditional normalizing flow [23] as the mechanism for each endogenous variable  $v_k := f_k(u_k; \mathbf{pa}_k)$ , to enable tractable and explicit abduction of the exogenous noise  $u_k = f_k^{-1}(v_k; \mathbf{pa}_k)$ . DSCMs can thereby tractably estimate counterfactuals given observed attributes and intervention(s). The counterfactual of any  $v_k$  is given by  $\widehat{v}_k := f_k(f_k^{-1}(v_k; \mathbf{pa}_k); \widehat{\mathbf{pa}}_k)$ , where  $\widehat{\mathbf{pa}}_k$  are the counterfactual parents of  $v_k$  resulting from an upstream intervention.

However, it has been shown that directly applying DSCMs [14] to 3D brain MRIs is impractical due to the complexity of constructing and optimizing invertible neural networks [27,23]. Therefore, we propose a method that operates in a low-dimensional latent space. We first use a Vector Quantized Variational Autoencoder (VQ-VAE) to learn a compressed latent representation of the MRIs. Within this space, our approach then adapts the Latent Structural Causal Model (LSCM) to separate the MRI variables ( $\mathbf{x}$ ) from other relevant variables ( $V$ , e.g., clinical or demographic data). We then utilize a Generalized Linear Model (GLM) [12] to perform the counterfactual steps, such as abduction and action. The GLM is well-suited for this task as it provides an interpretable, linear framework for modeling these causal interventions. After estimation of all counterfactual attributes, we obtain the counterfactuals of image latent features  $\mathbf{z}$ 's parents (see next section for details of  $\mathbf{z}$ ), i.e.  $\widehat{\mathbf{pa}}_{\mathbf{z}}$ , which will be used to generate  $\widehat{\mathbf{z}}$ . The resulting counterfactual feature encoding is converted into an MRI using the decoder of the VQ-VAE model.

## 2.2 Latent SCM for 3D Counterfactual MRIs

To fully leverage the latent SCM described in Section 2.1, a high-dimensional MRI  $\mathbf{x}$  first has to be encoded to a corresponding latent feature  $\mathbf{z}$ , for which we use a VQ-VAE. Then, we obtain its counterfactual  $\widehat{\mathbf{z}}$  based on  $\widehat{\mathbf{pa}}_{\mathbf{z}}$ , which is finally decoded to the MRI counterfactual  $\widehat{\mathbf{x}}$ . We now discuss the process of obtaining these latent features  $\mathbf{z}$  and estimating the counterfactuals  $\widehat{\mathbf{z}}$ , after which decoding is trivial given a trained VQ-VAE.

**Computing latent feature  $\mathbf{z}$ .** To obtain a latent feature  $\mathbf{z}$  from a 3D MRI  $\mathbf{x}$ , we employ a Variational Autoencoder (VQ-VAE) [13]. VQ-VAEs comprise an encoder  $\mathcal{E}$  and decoder  $\mathcal{D}$ , as well as a code book  $\mathcal{C}$  that performs vector quantisation (VQ). That is, code book  $\mathcal{C}$  empowers mapping a 3D MRI  $\mathbf{x}$  to a quantized encoding.

The first step in the process of computing the latent feature  $\mathbf{z}$  is using the encoder  $\mathcal{E}$  to map the 3D MRI  $\mathbf{x} \in \mathbb{R}^{D \times H \times W}$  to its lower-dimensional feature representation  $\mathbf{z} := \mathcal{E}(\mathbf{x}) \in \mathbb{R}^{d \times h \times w \times n_D}$ . Correspondingly, the decoder  $\mathcal{D}$  aims to reconstruct a 3D MRI  $\widehat{\mathbf{x}} = \mathcal{D}(\mathbf{z})$  from a compressed embedding  $\mathbf{z}$ . The training objective of the model is to minimize the reconstruction error. Once latent feature  $\mathbf{z}$  is obtained, we apply vector quantization, which discretizes the continuous latent space using a set of embedding units  $\mathcal{C} := \{(k, e(k)) : k = 1, 2, \dots, N_C \text{ and } e(k) \in \mathbb{R}^{n_D}\}$ . This allows an MRI to be represented very efficiently by a set of indices (a.k.a. code) as defined with respect to the code book.

Notably, this process also serves a regularization purpose to avoid overfitting the model during training.

After the encoding and vector quantization steps are finished, the latent representation  $\mathbf{z}$  is described by  $d \times h \times w$  vectors of  $n_D$  dimensions each. This is achieved by searching the nearest neighbor of the embedding units in codebook  $\mathcal{C}$  for each feature vector in  $z_c$ . In other words, each of the  $d \times h \times w$  vectors  $z_c \in \mathbb{R}^{n_D}$  from  $\mathbf{z}$  is paired with its closest representative  $e(k)$  from the codebook such that the corresponding code (a.k.a. index) is  $\mathcal{I}(z_c) := \arg \min_k (z_c - e(k))$ . Subsequently,  $e(\mathcal{I}(z_c))$  is the representative such that the quantization of the latent encoding may be formulated as  $Q(z_c) = [e(\mathcal{I}(z_c))]_{z \rightarrow \mathbf{z}}$ , where  $[\cdot]_{z \rightarrow \mathbf{z}}$  denotes the vectors  $z_c$  defined according to  $\mathbf{z}$ . Building on this foundation of vector quantization, we propose a fine-grained quantization process that acquires multiple quantizations per vector, namely the vector’s own quantization as well as the quantization of its residual. However, we first reshape the MRI’s latent encoding  $\mathbf{z} \in \mathbb{R}^{d \times h \times w \times n_D}$  to  $\mathbb{R}^{2 \times d \times h \times w \times \frac{n_D}{2}}$  so that  $\mathbf{z}$  consists of twice as many vectors  $z_h \in \mathbb{R}^{\frac{n_D}{2}}$  with half the size; in other words, each  $z_c \in \mathbb{R}^{n_D}$  gets split into two vectors  $z_h \in \mathbb{R}^{\frac{n_D}{2}}$ . For each of the vectors  $z_h$ , we determine the code  $\mathcal{I}(z_h)$  as done above (with  $e(k) \in \mathbb{R}^{\frac{n_D}{2}}$  also being half in size), and then compute the code corresponding to the residual, i.e.,  $\mathcal{I}(z_h - e(\mathcal{I}(z_h)))$ , so that the quantized encoding can be written as

$$Q(z_h) := e(\mathcal{I}(z_h)) + e(\mathcal{I}(z_h - e(\mathcal{I}(z_h)))). \quad (1)$$

For every  $z_c$  comprised of two  $z_h$ , we stack the two quantized encodings  $Q(z_h)$  to reconstruct a vector of the original size, thus obtain a quantized vector representation of  $\mathbf{z}$ , which is subsequently fed into the decoder.

**Estimate latent counterfactual  $\hat{\mathbf{z}}$  and  $\hat{\mathbf{x}}$ .** Given feature  $\mathbf{z} = Q(\mathcal{E}(\mathbf{x}))$ , we will build a closed-form mechanism  $f$  for  $\mathbf{z}$ , such that its exogenous variable is given by  $\mathbf{u}_{\mathbf{z}} = f_{\theta}^{-1}(\mathbf{p}_{\mathbf{a}_{\mathbf{z}}}, \mathbf{z})$ . We achieve this by using the GLM. Specifically, we first flatten the feature as a vector with dimension  $K = d \times h \times w \times n_D$ . Then, a feature matrix  $\mathbf{Z} \in \mathbb{R}^{N \times K}$  is built for all the  $N$  samples in the dataset. At the same time, the  $\mathbf{p}_{\mathbf{a}_{\mathbf{z}}}$  for all training samples is accumulated to construct a matrix  $\mathcal{P} \in \mathbb{R}^{N \times m}$ , where  $m$  is the number of variables in  $\mathbf{p}_{\mathbf{a}_{\mathbf{z}}}$ . Then, an ordinary least square estimator [12] is applied to solve the GLM’s normal equations so that the linear parameters  $\mathcal{B}$  can be represented by the closed-form solution

$$\mathcal{B} = (\mathcal{P}^T \mathcal{P})^{-1} \mathcal{P}^T \mathbf{Z}.$$

Subsequently, the **Abduction** step of the counterfactual generation can be represented as the computation of the residual component  $\mathbf{U}_{\mathbf{z}} \in \mathbb{R}^{N \times K}$  acting as the exogenous variable for features  $\mathbf{Z}$ , which is given by

$$\mathbf{U}_{\mathbf{z}} = \mathbf{Z} - \mathcal{P}\mathcal{B} = (\mathbf{I} - (\mathcal{P}^T \mathcal{P})^{-1} \mathcal{P}^T) \mathbf{Z}.$$

Given that we construct  $\mathcal{P}$  explicitly, we find that the solution for  $\mathcal{B}$ , and thus for  $\mathbf{U}_{\mathbf{z}}$ , is of closed-form. This is computationally feasible as we perform the

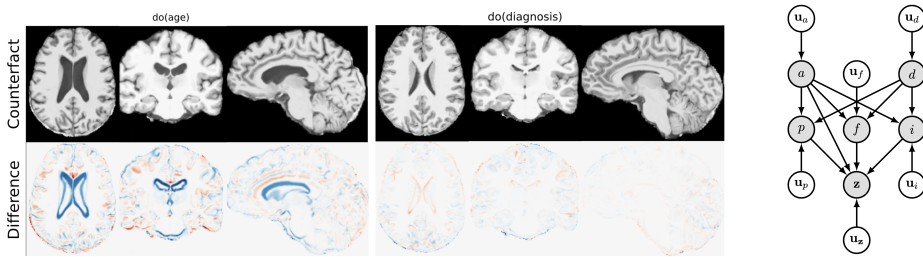


Fig. 2: Counterfactual cases. **Left:** the counterfactual and the differences with original input for each intervention. **Right:** The assumed causal graph is based on [25]. Variables in the graph are age ( $a$ ), diagnosis ( $d$ ), Parietal ( $p$ ), Frontal ( $f$ ), Insula ( $i$ ), and latent features of MRI ( $z$ ). Regarding the difference image, blue refers to negative and light orange to positive differences.

GLM in the latent space, not in the high-dimensional MRI space. Our method is scalable and easily lends itself to cases containing many more samples. Like metadata normalization [12], we can accumulate the  $\mathcal{B}$  with momentum.

The **Action** step of the counterfactual generation can be realized by using the causal graph to produce counterfactual parents  $\widehat{\mathbf{p}}\mathbf{a}_z$ . Once we have the  $\widehat{\mathbf{p}}\mathbf{a}_z$ , the **Prediction** step of counterfactual generation can be achieved by adding factor-specific embeddings back to the exogenous variable as follows:

$$\widehat{\mathbf{z}} = \mathbf{U}_z + \widehat{\mathcal{P}}\mathcal{B}.$$

By recovering its spatial resolution and decoding using the generator, we get the MRI counterfactual in the observation/MRI space, i.e.,  $\mathbf{x} = \mathcal{D}(\widehat{\mathbf{z}})$ ,  $\widehat{\mathbf{z}} \in \widehat{\mathbf{Z}}$ .

### 3 Experiments

We train and test our VQ-VAE model on 4583 t1-weighted brain MRIs of 1188 controls from two public datasets: the Alzheimer’s Disease Neuroimaging Initiative [20] (ADNI; 380 subjects, age range: 59 to 91 years, Data Releases: ADNI 1, 2, 3 and GO) and the National Consortium on Alcohol and Neurodevelopment in Adolescence [1] (NCANDA; 808 subjects, age at baseline: 12 to 21 years, maximum age: 27 years, Data Release: NCANDA\_PUBLIC\_6Y\_STRUCTURAL\_V01). Additional details about the two data sets are provided in [18]. We first define the test set by selecting the baseline MRIs of 400 subjects so that they are matched with respect to age and sex, i.e., we separate all samples into 20 groups based on their baseline age and then randomly select 10 females and 10 males for each age group. From the remaining 1919 subjects, we create a training set consisting of 4183 (baseline and follow-up) t1-weighted brain MRIs that is matched with respect to age and sex to the test set. Each MRI is processed using the pipeline described in [18], which includes denoising, bias field correction, skull stripping, affine registration to a template (which corrects for difference in head size and

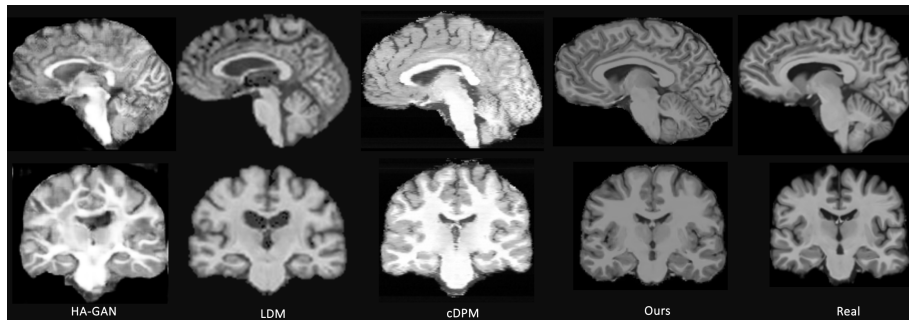


Fig. 3: 2 views of real MRI vs synthetic MRIs generated by 4 models. Our model can produce visually similar MRI to others but we can do counterfactual generation.

thus sex and race), and normalizing intensity values between 0 and 1. The voxel resolution is 1mm and we pad each MRI to spatial resolution  $144 \times 176 \times 144$ .

Once training is completed, we freeze the VQ-VAE and train and test the Deep Structural Causal Model (DSCM) on an in-house dataset (PIs: Drs. Pfefferbaum and Sullivan) of 826 T1-weighted MRIs from 421 subjects (age: 25 to 75 years) using five-fold cross-validation. 199 of the 421 subjects are diagnosed with alcohol use disorder (AUD) while the rest are healthy controls. According to [25], the volumes of the frontal, insula, and parietal lobes are smaller in those with AUD (compared to controls). Therefore, we build our casual graph, as in Fig. 2, based on the five variables age, diagnosis, frontal volume, insula volume, and parietal volume. We evaluate the model with respect to its ability to create counterfactuals and the anatomical plausibility of the synthetic 3D MRIs.

### 3.1 Counterfactual Generation

Fig. 2 shows an example of two 3D counterfactuals generated by our approach when applying an intervention  $do()$  to age and diagnosis in our causal graph. According to this figure, our model demonstrates a strong counterfactual generation ability with high fidelity. Intervention on diagnosis reveals a global but subtle changes on the brain. For the age intervention, we can see clear changes in the ventricle, a region known to be significantly influenced by the aging process.

### 3.2 Counterfactual Evaluation

We created 400 counterfactuals using random interventions. Using the same training setup, we then visually compare one of its generated MRIs to that of the best three baseline approaches according to [18], i.e., HA-GAN [26] and the diffusion models latent diffusion model (LDM) [21] and cDPM [17]). Afterwards, we evaluate its anatomical plausibility as described in [18].

According to Fig. 3, HA-GAN was the only method that did not produce MRIs that looked like those of healthy controls. LDM produces the most noisy

Table 1: Subcortical, Cerebellum, and ventricular regions. Cohen’s  $d$  is reported here as the effect size (**Effect**). 50% of the **ROIs** show strong correlations with the real data as  $|d| < 0.2$ .

<b>ROI</b>	vessel	5th	optic	accumbens	choroid	cc_mid	cc	cc_mid
	volume	ventricle	chiasm	area	plexus	posterior	central	anterior
<b>Effect</b>	0.0065	-0.0547	-0.4014	-0.0028	0.2400	0.2540	-0.3216	-0.1132
<b>ROI</b>	cc	cc	3rd	amygdala	4th	pallidum	WM	caudate
	anterior	posterior	ventricle		ventricle		hypo.	
<b>Effect</b>	0.3581	0.3939	-0.1804	-0.1686	-0.3383	0.5588	-0.0417	-0.1362
<b>ROI</b>	hippo	putamen	ventraldc	thalamus	lateral	brain	cerebellum	cerebellum
	campus				ventricle	stem	WM	cortex
<b>Effect</b>	0.2833	-0.1373	0.6070	0.3978	0.1306	0.2529	0.1690	-0.0748

MRI and the MRI of cDPM has clear slice artefacts. In contrast, the MRI of our model shows clear gray matter boundaries and looks most similar to the real MRI. Finally, our model is a one-step approach, which is much faster than the diffusion-based method as there is no need for the multi-step diffusion process.

We evaluate the anatomical plausibility of the MRIs produced by our method by comparing the similarity of their subcortical, cerebellum, and ventricle regions with the real data from ADNI and NCANDA. To this end, we run the Freesurfer pipeline [5] for both of the 400 real samples and the synthetic ones to obtain the brain parcellations and corresponding volumes of brain regions (recorded in ‘aseg’ by Freesurfer). We report the effect size of the volume scores of those 24 regions (using Cohen’s  $d$  coefficient [2],  $d$ ) with respect to the real brain MRIs. As shown in Table 1, 50% of the regions have a  $|d| < 0.2$ , which means these brain regions are very similar to the real ones. More than 90% of the 24 brain regions have an effect size that is less than 0.4, which suggests that the observed difference between the real and synthetic is relatively minor or subtle.

## 4 Conclusion

We propose a novel brain counterfactual for 3D MRI generation, which fully fills three rungs of Pearl’s ladder of causation. The model adeptly performs causal modeling while capable of generating high-quality 3D brain volumes. This is achieved by our latent structural counterfactual model, which contains a deep SCM constructed in a latent space. We then run a GLM on this low dimensional latent space to synthesize counterfactuals, to mitigate significant computational challenges posed by performing interventions directly on the 3D brain MRIs. The generated MRIs show high anatomical resolution, while the counterfactual generation contains an efficient intervention strategy to generate high-quality 3D counterfactuals.

## 5 Acknowledgement

Collection and distribution of the NCANDA data were supported by NIH funding AA021681, AA021690, AA021691, AA021692, AA021695, AA021696, AA021697. Access to NCANDA data is available via the NIAAA Data Archive, collection 4513 ([https://nda.nih.gov/edit\\_collection.html?id=4513](https://nda.nih.gov/edit_collection.html?id=4513)).

This work was partly supported by funding from the National Institute of Health (MH113406, DA057567, AG084471, AA021697, AA017347, AA010723, AA005965, and AA028840), the DGIST R&D program of the Ministry of Science and ICT of KOREA (22-KUJoint-02), Stanford School of Medicine Department of Psychiatry and Behavioral Sciences Faculty Development and Leadership Award, the Stanford HAI-Google Research Collaboration, the Stanford HAI Google Cloud Credits, the 2024 Stanford HAI Hoffman-Yee Grant, and the UKRI AI programme, and the Engineering and Physical Sciences Research Council, for CHAI - EPSRC Causality in Healthcare AI Hub (grant no. EP/Y028856/1).

## References

1. Brown, S.A., Brumback, T., Tomlinson, K., Cummins, K., Thompson, W.K., Nagel, B.J., De Bellis, M.D., Hooper, S.R., Clark, D.B., Chung, T., Hasler, B.P., Colrain, I.M., Baker, F.C., Prouty, D., Pfefferbaum, A., Sullivan, E.V., Pohl, K.M., Rohlfing, T., Nichols, B.N., Chu, W., Tapert, S.F.: The National Consortium on Alcohol and Neurodevelopment in Adolescence (NCANDA): a multisite study of adolescent development and substance use. *Journal of Studies on Alcohol and Drugs* **76**(6), 895–908 (2015)
2. Cohen, J.: *Statistical power analysis for the behavioral sciences*. Academic press (2013)
3. De Sousa Ribeiro, F., Xia, T., Monteiro, M., Pawlowski, N., Glocker, B.: High fidelity image counterfactuals with probabilistic causal models. In: *Proceedings of the 40th International Conference on Machine Learning*. *Proceedings of Machine Learning Research*, vol. 202, pp. 7390–7425 (23–29 Jul 2023), <https://proceedings.mlr.press/v202/de-sousa-ribeiro23a.html>
4. De Sousa Ribeiro, F., Xia, T., Monteiro, M., Pawlowski, N., Glocker, B.: High fidelity image counterfactuals with probabilistic causal models. *ICML* (2023)
5. Fischl, B.: Freesurfer. *NeuroImage* **62**(2), 774–781 (2012)
6. Ho, J., Jain, A., Abbeel, P.: Denoising diffusion probabilistic models. *Advances in Neural Information Processing Systems* **33**, 6840–6851 (2020)
7. Jung, E., Luna, M., Park, S.H.: Conditional GAN with an attention-based generator and a 3D discriminator for 3D medical image generation. In: *International Conference on Medical Image Computing and Computer-Assisted Intervention*, *Lecture Notes in Computer Science*. vol. 12906, pp. 318–328 (2021)
8. Jung, E., Luna, M., Park, S.H.: Conditional GAN with 3D discriminator for MRI generation of Alzheimer’s disease progression. *Pattern Recognition* **133**, 109061 (2023)
9. Karras, T., Laine, S., Aila, T.: A style-based generator architecture for generative adversarial networks. In: *IEEE/CVF Conference on Computer Vision and Pattern Recognition*. pp. 4401–4410 (2019)

10. Kwon, G., Han, C., Kim, D.s.: Generation of 3D brain MRI using auto-encoding generative adversarial networks. In: International Conference on Medical Image Computing and Computer-Assisted Intervention, Lecture Notes in Computer Science. vol. 11766, pp. 118–126 (2019)
11. La Barbera, G., Boussaid, H., Maso, F., Sarnacki, S., Rouet, L., Gori, P., Bloch, I.: Anatomically constrained CT image translation for heterogeneous blood vessel segmentation. In: British Machine Vision Virtual Conference. p. 776 (2022)
12. Lu, M., Zhao, Q., Zhang, J., Pohl, K.M., Fei-Fei, L., Niebles, J.C., Adeli, E.: Metadata normalization. In: IEEE/CVF Conference on Computer Vision and Pattern Recognition. pp. 10917–10927 (2021)
13. van den Oord, A., Vinyals, O., Kavukcuoglu, K.: Neural discrete representation learning. In: Advances in Neural Information Processing Systems. pp. 6309–6318 (2017)
14. Pawlowski, N., Coelho de Castro, D., Glocker, B.: Deep structural causal models for tractable counterfactual inference. In: Advances in Neural Information Processing Systems. vol. 33, pp. 857–869 (2020)
15. Pawlowski, N., Coelho de Castro, D., Glocker, B.: Deep structural causal models for tractable counterfactual inference. *Advances in Neural Information Processing Systems* **33**, 857–869 (2020)
16. Pearl, J.: *Causality*. Cambridge university press (2009)
17. Peng, W., Adeli, E., Bosschieter, T., Park, S.H., Zhao, Q., Pohl, K.M.: Generating realistic brain mris via a conditional diffusion probabilistic model. In: International Conference on Medical Image Computing and Computer-Assisted Intervention, Lecture Notes in Computer Science. vol. 14227, pp. 14–24. Springer (2023)
18. Peng, W., Bosschieter, T., Ouyang, J., Paul, R., Sullivan, E.V., Pfefferbaum, A., Adeli, E., Zhao, Q., Pohl, K.M.: Metadata-conditioned generative models to synthesize anatomically-plausible 3D brain MRIs. *Medical Image Analysis* **98**, 103325 (2024)
19. Peters, J., Janzing, D., Schölkopf, B.: *Elements of causal inference: foundations and learning algorithms*. The MIT Press (2017)
20. Petersen, R.C., Aisen, P.S., Beckett, L.A., Donohue, M.C., Gamst, A.C., Harvey, D.J., Jack, C.R., Jagust, W.J., Shaw, L.M., Toga, A.W., Trojanowski, J., Weiner, M.: Alzheimer’s Disease Neuroimaging Initiative (ADNI): clinical characterization. *Neurology* **74**(3), 201–209 (2010)
21. Pinaya, W.H., Graham, M.S., Kerfoot, E., Tudosiu, P.D., Dafflon, J., Fernandez, V., Sanchez, P., Wolleb, J., da Costa, P.F., Patel, A., et al.: Generative AI for medical imaging: extending the MONAI framework. arXiv preprint arXiv:2307.15208 (2023)
22. Pinaya, W.H., Tudosiu, P.D., Dafflon, J., Da Costa, P.F., Fernandez, V., Nachev, P., Ourselin, S., Cardoso, M.J.: Brain imaging generation with latent diffusion models. In: Deep Generative Models, Lecture Notes in Computer Science. vol. 13609, pp. 117–126 (2022)
23. Rezende, D., Mohamed, S.: Variational inference with normalizing flows. In: International Conference on Machine Learning. pp. 1530–1538. Proceedings of Machine Learning Research (2015)
24. Sohl-Dickstein, J., Weiss, E., Maheswaranathan, N., Ganguli, S.: Deep unsupervised learning using nonequilibrium thermodynamics. In: International Conference on Machine Learning. pp. 2256–2265 (2015)
25. Sullivan, E.V., Zahr, N.M., Sassoon, S.A., Thompson, W.K., Kwon, D., Pohl, K.M., Pfefferbaum, A.: The role of aging, drug dependence, and hepatitis c comorbidity in alcoholism cortical compromise. *JAMA Psychiatry* **75**(5), 474–483 (2018)

26. Sun, L., Chen, J., Xu, Y., Gong, M., Yu, K., Batmanghelich, K.: Hierarchical amortized GAN for 3D high resolution medical image synthesis. *IEEE Journal of Biomedical and Health Informatics* **26**(8), 3966–3975 (2022)
27. Tabak, E.G., Vanden-Eijnden, E.: Density estimation by dual ascent of the log-likelihood. *Communications in Mathematical Sciences* **8**(1), 217–233 (2010)
28. Wolleb, J., Bieder, F., Sandkühler, R., Cattin, P.C.: Diffusion models for medical anomaly detection. In: *International Conference on Medical Image Computing and Computer-Assisted Intervention, Lecture Notes in Computer Science*. vol. 13438, pp. 35–45 (2022)
29. Xia, K.M., Pan, Y., Bareinboim, E.: Neural causal models for counterfactual identification and estimation. In: *The Eleventh International Conference on Learning Representations (2023)*, <https://openreview.net/forum?id=vouQcZS8KfW>
30. Xing, S., Sinha, H., Hwang, S.J.: Cycle consistent embedding of 3d brains with auto-encoding generative adversarial networks. In: *Medical Imaging with Deep Learning (2021)*, <https://openreview.net/forum?id=jgBzGIG-kB>
31. Zhao, Q., Liu, Z., Adeli, E., Pohl, K.M.: Longitudinal self-supervised learning. *Medical Image Analysis* **71**, 102051 (2021)
32. Zheng, S., Charoenphakdee, N.: Diffusion models for missing value imputation in tabular data. In: *NeurIPS Table Representation Learning (TRL) Workshop (2022)*